Catalysis Today 172 (2011) 232–239

Contents lists available at ScienceDirect

Catalysis Today

journal homepage: www.elsevier.com/locate/cattod

Hydrodeoxygenation of 2-methoxyphenol over Mo_2N catalysts supported on activated carbons

C. Sepúlveda[a], K. Leiva[a], R. García[a], L.R. Radovic[b,c], I.T. Ghampson[d], W.J. DeSisto[d,*], J.L. García Fierro[e], N. Escalona[a,*]

[a] Universidad de Concepción, Facultad de Ciencias Químicas, Edmundo Larenas 129, Casilla 160C, Chile
[b] Universidad de Concepción, Facultad de Ingeniería, Edmundo Larenas 215, Concepción, Chile
[c] Penn State University, Department of Energy and Mineral Engineering, University Park, PA 16802, USA
[d] University of Maine, Department of Chemical & Biological Engineering, Orono, ME 04469, USA
[e] Instituto de Catálisis y Petroquímica, CSIC, Cantoblanco, 28049 Madrid, Spain

ARTICLE INFO

Article history:
Received 30 November 2010
Received in revised form 26 January 2011
Accepted 18 February 2011
Available online 9 April 2011

Keywords:
HDO
2-Methoxyphenol
Mo_2N
Carbon support

ABSTRACT

The hydrodeoxygenation (HDO) of 2-methoxyphenol using Mo_2N supported on three commercial activated carbons (Pica, Norit and Cudu) with different textural and chemical properties was studied. The reaction was carried out in a batch reactor at 50 bar of H_2 and 300 °C. The catalysts were prepared by wetness impregnation and nitrided with ammonia at 700 °C. The supports and catalysts were characterized by N_2 adsorption–desorption, thermal programmed desorption (TPD), X-ray photoelectron spectroscopy (XPS), X-ray fluorescence and X-ray diffraction (XRD). The Mo_2N/Norit catalyst displayed higher HDO activity compared to the Mo_2N/Cudu and Mo_2N/Pica catalysts. HDO conversion increased when the Mo_2N/Norit catalysts were activated with hydrogen for 6 h at 400 °C due to increased surface nitridation. The Mo_2N/Norit catalyst displayed a higher phenol/catechol ratio relative to the Mo_2N/Pica and Mo_2N/Cudu catalysts, which displayed similar (phenol/catechol) ratios. The phenol/catechol ratio was unaffected by the H_2 activation time.

1. Introduction

The transportation sector accounts for more than 30% of the energy consumption in the European Union, and consumption is continuously increasing [1]. Currently, the price of oil and natural gas is highly volatile, with a clear upward trend due to the demand of rapidly developing countries such as China, India and Brazil. This, combined with CO_2 emissions from fossil fuels, has attracted renewed interest in the development of new, renewable energy technologies. Many researchers have focused their attention on the transformation of biomass to transportation fuels and chemicals because biomass is both a renewable resource and inert with respect to CO_2 emissions [2–8].

Biomass may be gasified to biosyngas and then converted to liquid fuels and/or gases by Fischer Tropsch Synthesis (FTS) [9–13]. Biomass can also by pyrolyzed and converted to primarily liquid and solid products. The liquid is called pyrolysis oil or bio-oil. It is brown and viscous with a high oxygen content due to the presence of large quantities of oxygenates. These are reactive and can polymerize, resulting in a product that is unstable. In addition, bio-oil is not miscible with diesel and has a low heating value. Efforts at developing catalytic hydrotreating processes to remove oxygen (hydrodeoxygenation or HDO) and improve the chemical and fuel properties of bio-oil are critical to its eventual use as a transportation fuel [14,15].

Laurent and Delmon [16,17] reported the HDO of a model compound mixture representing bio-oil over CoMo/γ-Al_2O_3 and NiMo/γ-Al_2O_3 catalysts. In particular, 2-methoxyphenol (guaiacol) is an excellent model compound for bio-oil that contains two oxygen functionalities (–OH and –OCH_3) [3–6]. They found that guaiacol first underwent a demethylation (DME) forming catechol. Catechol was subsequently deoxygenated by a combination of C–O bond breaking (DDO) and hydrogenation (HYD). The final products were benzene and cyclohexane, as shown in Fig. 1. Sulfided CoMo/Al_2O_3 and NiMo/Al_2O_3 catalysts used in these HDO experiments were industrial hydrodesulfurization (HDS) catalysts and have been reported to be useful also for HDO [18–20]. As an example of alternative HDO catalysts, Ruiz et al. [21] recently studied rhenium sulfides supported on zirconia and sulfided zirconia. They found that guaiacol HDO activity of ReS_2/ZrO_2 increased 6.4 times when sulphided in a H_2S/N_2 mixture. Similar behavior has been observed in the HDS of thiophene [22].

* Corresponding authors.
E-mail addresses: WDeSisto@umche.maine.edu (W.J. DeSisto), nescalona@udec.cl (N. Escalona).

0920-5861/$ – see front matter © 2011 Elsevier B.V. All rights reserved.
doi:10.1016/j.cattod.2011.02.061

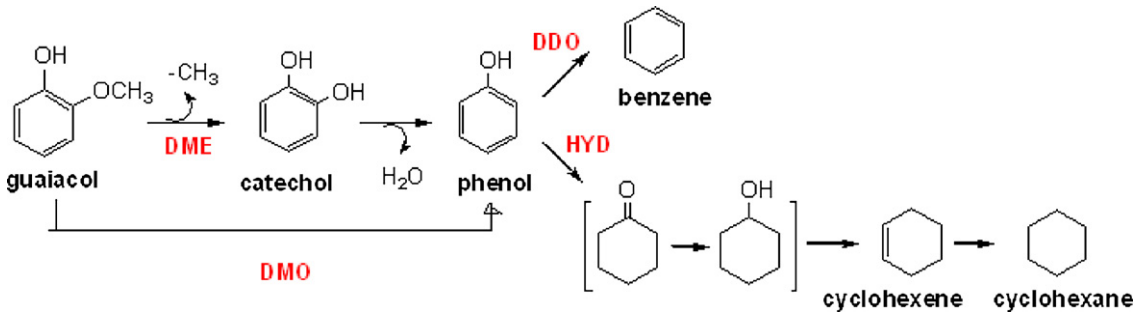

Fig. 1. HDO reaction scheme for guaiacol conversion.

Although transition metal sulfide catalysts have been effective for HDO of bio-oil, they suffer from deactivation during reaction processing [23–26]. In order to maintain active sulfided catalysts, small amounts of H_2S must be added to the feed. Alternatively, Bui et al. [20] have shown a new and interesting method for co-processing bio-oil with gas-oil, simultaneously performing HDS and HDO to maintain a stable active catalyst phase for HDO.

In addition to metal sulfides, metal nitrides have shown to be stable and active for HDS [27,28]. Considering that HDS catalysts are suitable for HDO, it is expected that metal nitride/support phases would also display a high activity for HDO. Recently, Monnier et al. [29] studied the HDO of oleic acid and canola oil over alumina-supported metal nitrides. They found that activated phases of WN, VN and Mo_2N displayed a high activity, with Mo_2N achieving the highest formation of alkanes. In this study, we report the synthesis and characterization of molybdenum nitride catalysts supported on activated carbons; the potential advantages of carbon as a support are well known [30]: (i) in HDS reactions its acidity can be tailored to minimize cracking [31]; (ii) it can be produced inexpensively from the solid product of biomass pyrolysis; and (iii) its surface physical and chemical properties can be tailored over wide ranges in this process [32]. The effects of the support and of the catalyst activation conditions were evaluated in the HDO of guaiacol.

2. Experimental

2.1. Preparation of catalysts

The supported molybdenum oxide catalysts were prepared by wetness impregnation using aqueous solutions of ammonium heptamolybdate [$(NH_4)\,6Mo_7O_{24}{\cdot}4H_2O$, Fisher Scientific] as a precursor salt. Three commercial activated carbons (Pica PICATAL, Norit Darco® MRX and Cudu PETROCHIL), whose textural properties are summarized in Table 1, were used as supports. After impregnation, the samples were dried at 110 °C for 12 h and calcined at 500 °C for 4 h. The catalysts were prepared to obtain a nominal loading of 10 wt% Mo. An unsupported molybdenum oxide precursor was prepared by thermal decomposition of ammonium heptamolybdate at 500 °C for 4 h. The nitrides were prepared following the procedure described by Volpe and Boudart [33]. This procedure involved a temperature-programmed reaction of the molybdenum oxide precursor with ammonia (100 mL min^{-1}). The temperature was linearly increased from room temperature to 300 °C in 30 min, 300–500 °C in 330 min, and 500 to 700 °C in 100 min. It was maintained at 700 °C for 2 h. The samples were then cooled under ammonia flow to room temperature and passivated with O_2/N_2 1% for 12 h. Prior to reaction, the catalysts were activated in hydrogen at various temperatures and times. The catalysts were stored in nitrogen prior to use.

2.2. Reaction conditions

HDO of guaiacol was carried out using a batch reactor (model Parr 4841). The feed contained 0.232 mol L^{-1} guaiacol, hexadecane as internal standard (0.0341 mol L^{-1}) and 100 mL of decalin as solvent. Prior to reaction the catalysts (0.2 g) were reduced ex-situ at 400 °C for 4 h with a flow of H_2 (4 L h^{-1}). To avoid air contamination, N_2 was bubbled through the solution for 1 h. The reactor was then heated under N_2 up to the reaction temperature, 300 °C, under continuous stirring. N_2 was then replaced by H_2 and the reactor was pressurized to 5 MPa, which was kept at constant during the course of the experiment. Samples were taken periodically during the reaction and analyzed by gas chromatography (GC) in a Perkin Elmer Autoystem XL. The reaction rates were calculated from the initial slopes of the conversion data. The phenol/cathecol ratio was determined at 3% conversion of guaiacol.

2.3. Characterization of supports and catalysts

The "apparent" surface area, micropore and mesopore volume and average pore diameter of the supports and catalysts were determined from nitrogen isotherms at −196 °C using a Micromeritics ASAP-2020 instrument. Prior to the measurements, the samples were degassed at 200 °C for 12 h. The total micro-plus mesopore volumes of the materials were calculated from the amount adsorbed at a relative pressure of 0.99 on the desorption branch of the corresponding isotherms, equivalent to the filling of all pores below 50 nm diameter. The contribution of micropores was calculated from a *t-plot* analysis of these isotherms, where the intercept of the linear portion was equivalent to the micropore volume and the slope proportional to the external surface area. The mesopore volume was obtained by subtracting the *t-plot* micropore volume

Table 1
Specific surface (S_{BET}), micropore volume (V_o), mesopore volume (V_m) and average pore diameter of the catalysts and supports, and zero point charge (pH) of the activated carbon supports.

Sample	S_{BET} ($m^2\,g^{-1}$)	V_o ($cm^3\,g^{-1}$)	V_m ($cm^3\,g^{-1}$)	Pore diameter (nm)	Zero point charge (pH)
Norit	612	0.12	0.50	7.9	6.88
MoO_3/Norit	479	0.08	0.46	8.2	
Mo_2N/Norit	752	0.14	0.58	7.9	
Pica	1181	0.41	0.16	4.3	6.81
MoO_3/Pica	1072	0.31	0.2	4.4	
Mo_2N/Pica	1213	0.31	0.32	5.0	
Cudu	1057	0.33	0.18	5.0	7.81
MoO_3/Cudu	741	0.23	0.12	4.8	
Mo_2N/Cudu	811	0.23	0.19	4.9	
Unsupported			–		–
MoO_3	3.0	–		–	
Mo_2N	1.6	–	–	–	

from the total pore volume. The average pore diameter was calculated from the desorption branch of the isotherm using the BJH method.

Temperature-programmed desorption (TPD) analysis of the activated carbons was carried out under inert atmosphere at 10 °C/min and a helium flow of 50 mL min^{-1}. The quantity of gases evolved (CO_2 and CO combined) was measured using a thermal conductivity detector (TCD).

X-ray photoelectron spectra (XPS) of reduced catalysts were obtained on an Escalab 200R electron spectrometer using a Mg Kα (1253.6 eV) photon source. The catalyst samples were pre-reduced ex-situ with H_2 at 400 °C for 4 h. After reduction, the samples were cooled to room temperature, flushed with He and stored in flasks containing iso-octane, then transferred to the pre-treatment chamber of the spectrometer. The binding energies (BE) were referenced to the C 1s level of the carbon support at 284.9 eV. An estimated error of +0.1 eV can be assumed for all measurements. Intensities of the peaks were calculated from the respective peak areas after background subtraction and spectrum fitting by a combination of Gaussian/Lorentzian functions. Relative surface atomic ratios were determined from the corresponding peak intensities, corrected with tabulated sensitivity factors, with a precision of 7%.

X-ray diffraction (XRD) data were collected on a PANanalytical PRO X-ray diffractometer, using Cu radiation (λ = 1.54 Å) with Ni filter. Scans were collected between 10 and 85° 2θ at 0.02° s^{-1}. A sample mass of 0.050 g was placed in a quartz sample holder for measurement.

X-ray fluorescence data were collected on a Rigaku 3270 apparatus with a rhodium tube. Prior to analysis, the sample was emulsified in water and allowed to dry at room temperature. The sample mass was 0.020 g, placed in a quartz sample holder for measurement.

The Zero Point Charge (ZPC) of the three carbons was determined using the ASTM method D3838-05. Approximately 40 mL of distilled hot water was added to carbon in a flask. The flask was heated on a hot plate and a thermometer was used to ensure that no false boiling, due to trapped gases, occurred. The flask was then removed from the hot plate and its contents were filtered immediately through pre-moistened filter paper. The pH measurement was made at 50 ± 5 °C.

3. Results and discussion

3.1. Characterization of supports and catalysts

Table 1 summarizes the surface area (S_{BET}), micropore volume (V_o), mesopore volumes (V_m) and pore diameter information on the catalysts and the activated carbon (AC) supports. The three supports are seen to have distinctly different textural properties. The micropore volume of the Norit AC accounts for about 19% of its total pore volume while those of Pica and Cudu supports account, respectively, for 71 and 64%. The average pore diameters of the supports and catalysts were all in the mesopore range, with Norit AC-based materials having the largest pore diameter. After the catalyst precursor impregnation and calcination, the surface area and micropore volume decreased. The pore diameter for the Mo_2N/Cudu catalysts remained largely unchanged compared to their supports.

Table 1 also shows that impregnation of the Norit AC produced an increase in the average pore diameter of the support, suggesting that the active phase blocks the micropores of the support, shifting the distribution of pores to higher values (mesoporosity); however, the average pore diameter decreased upon nitriding of the MoO_x/Norit catalyst, accompanied by an increase in micro-and mesopore volumes. Such behavior suggests that during nitriding

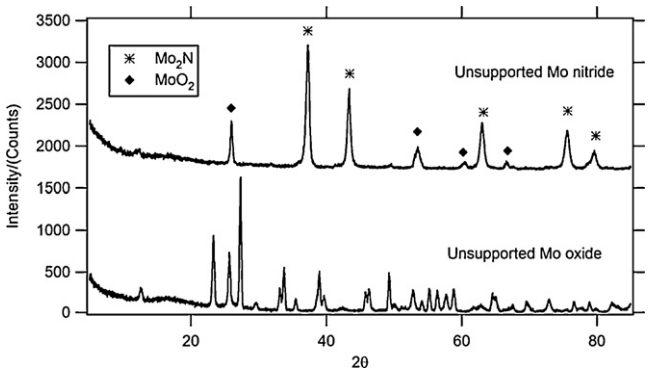

Fig. 2. XRD patterns for unsupported Mo oxide and nitride.

there is an additional activation of the Norit AC, thereby creating additional porosity. The Cudu and Pica supports did not display such a trend. These differences in behavior can be attributed to the abundant impurities in the Norit AC, as evidenced by its XRD pattern and fluorescence analysis.

Fig. 2 shows the X-ray diffraction patterns of the unsupported MoO_3 and Mo_2N used as a reference. The ammonium heptamolybdate precursor was completely transformed to MoO_3 during calcination. When the bulk, unsupported MoO_3 underwent nitridation, two different crystalline phases were observed, indicating that the conversion to nitride was incomplete. Diffraction peaks at 2θ = 37.6, 43.1, 64.1, 75.5 and 78.1 were assigned to Mo_2N (JCPDS 25-1368) and peaks at 2θ = 27.3, 53.1, 60.1 and 66.6 were assigned to MoO_2 (JCPDS 48-0123).

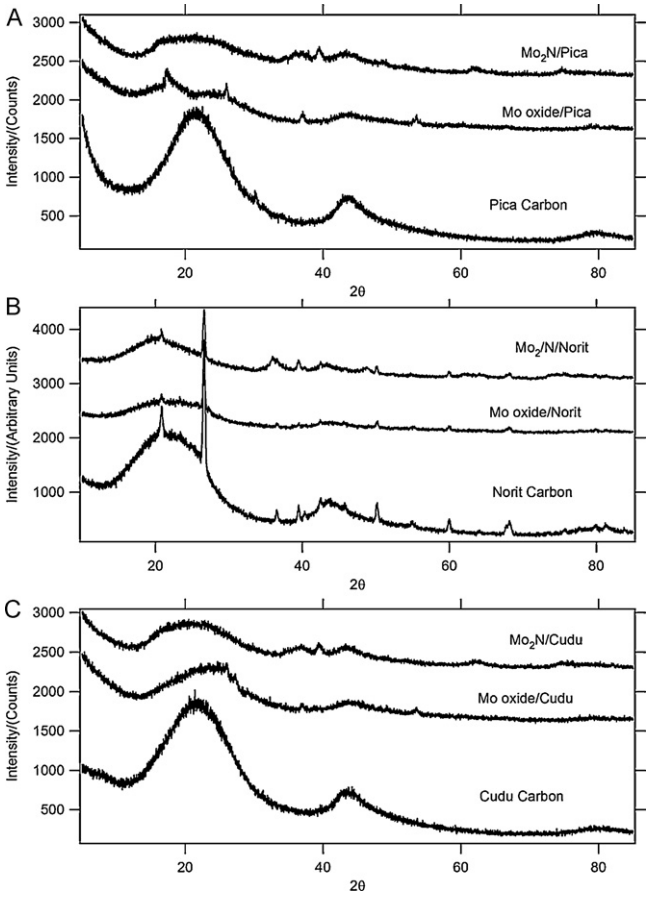

Fig. 3. XRD patterns for carbon-supported Mo oxides and nitrides: (a) Pica carbon, (b) Norit carbon and (c) Cudu carbon.

Fig. 3 shows the XRD patterns of the unloaded supports, the oxidized molybdenum precursor/support and the nitrided molybdenum/support materials. The oxidized Mo/Pica catalyst is seen to contain MoO_3 with peaks at $2\theta = 17.0$, 27.3, 37.2 and 53.0 (JCPDS 48-0123). Also, the peaks at about 35, 39 and 61° for some Mo_2N/C catalysts are attributed to impurities present in the supports. After nitriding, however, the presence of Mo_2N was not observed by XRD, indicating a re-dispersion of the catalyst on the support. No crystalline phases of molybdenum were detected on either the Norit- or Cudu-supported catalysts; this indicates a high degree of dispersion of the active phase on the support. An abundance of crystalline inorganic constituents is evident in the Norit AC support. These could be associated with the Ti and Sr impurities identified by XRF, or $CaCO_3$ identified by XRD.

Fig. 4 shows the TPD profiles of the three supports. Only Norit and Cudu had a very pronounced peak at low temperatures (250–400 °C), while the Cudu AC exhibited also a shoulder at 600–800 °C. Also, all the supports displayed a high-temperature peak at ca. 800–1000 °C. The peaks at 250–400 °C, 600–800 °C and 800–1000 °C are assigned mainly to carboxylic, phenolic or anhydride and quinone functional groups, respectively [34,35]. This is consistent with assignments reported previously by Figueiredo et al. [36]. Therefore, the Norit and Cudu supports contain strong acidic sites (which release CO_2 during decomposition of surface carboxyl groups), while all three supports contain weakly acidic sites associated with quinone-type surface functionalities (which release CO upon thermal decomposition).

The surface charge titration results (see Table 1) indicate that the Cudu AC is basic (PZC = 7.81), while the Pica (PZC = 6.81) and Norit (PZC = 6.88) supports are less so. The higher PZC value for the Cudu AC is in agreement with the TPD profiles, and confirms that its surface chemistry is different from that of the other two supports.

The XPS results for the reduced Mo_2N supported catalysts are summarized in Table 2, along with data obtained for the Mo_2N/Norit catalyst prepared under different reduction conditions. In all cases the XPS spectra (not shown) exhibited two doublets belonging to Mo $3d_{5/2}$ and $3d_{3/2}$ levels. The $3d_{5/2}$ energy at 229.0 eV, corresponding to Mo with an oxidation state between +4 and +2, is assigned to Mo_2N species [37]; the 230.9 eV peak is due to the presence of molybdenum oxynitrides similar to that reported previously for chromium oxynitrides [38]. The relative abundance (shown in parentheses) is also of interest: the Mo_2N/Cudu catalyst displayed the lower values, while the Mo_2N/Pica and Mo_2N/Norit catalysts displayed similar values. This result suggests that the Mo_2N/Cudu catalyst contained smaller amounts of Mo_2N species on the surface of the support. These observations in turn indicate

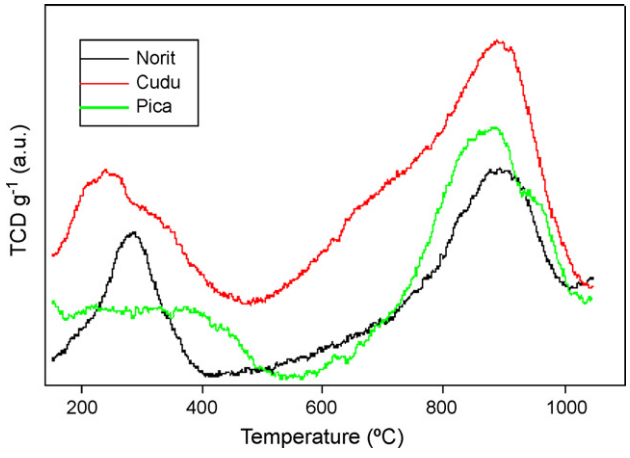

Fig. 4. TPD profiles for Norit, Cudu and Pica activated carbon supports.

Table 2
XPS binding energies (eV) and surface atomic ratios of nitrided catalysts.

Catalysts	Mo3d (eV)	N1s (eV)	C 1s (eV)	(Mo/C) at.	(Mo/N) at.
Mo_2N unsupport	229.0(69) 230.9(31)	394.9(58) 397.6(42)			0.81
Mo_2N/Cudu	229.1 (56) 231.6(44)	394.9(49) 397.7(51)	284.8(74) 286.4(18) 287.6(5) 289.4(3)	0.028	0.67
Mo_2N/Pica	229.2(62) 231.6(38)	394.9(37) 397.4(41) 400.0(22)	284.8(65) 286.4(22) 287.7(4) 289.4(9)	0.020	0.82
Mo_2N/Norit	229.3 (62) 231.5(38)	394.8(41) 397.3(42) 400.0(17)	284.8(71) 286.4(17) 287.7(6) 289.3(6)	0.024	0.66
Mo_2N/Norit (6 h)	229.3(68) 231.8 (32)	394.9(41) 397.3(41) 400.2(18)	284.8(72) 286.4(17) 287.7(7) 289.3(4)	0.022	0.68
Mo_2N/Norit (8 h)	229.2(60) 231.8(40)	394.9(47) 394.5(39) 400.2(14)	284.8(66) 286.3(21) 287.6(8) 289.4(5)	0.023	0.85

that, under the conditions used, the reduction of supported Mo oxide species was not complete, probably due to stronger interactions of the Mo oxide species with the more abundant surface oxygen groups of the Cudu support [39]. In contrast, when the Mo_2N/Norit catalyst was reduced for 6 h, the relative amount of Mo_2N species increased. Further increasing the reduction time to 8 h led to additional reduction, suggesting that the active phase is sensitive to activation conditions.

As can be seen in Table 2, the catalysts displayed four C 1s peaks between 284.8 and 289.4 eV. The binding energy at 284.8 eV is assigned to C–C and/or C=C bonds of aromatic and aliphatic carbon [34,40], and that at 286.4 eV to C–O bonds [41] in phenolic or ether groups [42], but also to C=N bonds [43]. The 287.6 eV peak is assigned to quinone-type groups or C=N species [43,44], and that at 289.4 eV to carboxyl groups and esters [42].

Table 2 also shows that all catalysts displayed two N 1s peaks. The binding energies at 394.9 eV and 397.5 eV correspond to two oxidation states of nitrogen assigned to Mo_2N species. [45,46]. Additionally, the Mo_2N/Pica and Mo_2N/Norit catalysts display another N 1s peak near 400.1 eV; it is assigned to a C=N bond corresponding to pyrrolic groups, as reported by Chowdhury et al. [47]; we thus infer that the higher concentration of oxygen surface groups on the Mo_2N/Cudu catalyst prevents the formation of such nitrided groups.

The Mo/C and Mo/N surface atomic ratios for each of the three catalysts, including those prepared under different activation conditions (Mo_2N/Norit), were calculated from XPS data and are also shown in Table 2. The Mo_2N/Pica catalyst displayed the lowest Mo/C ratio, while the Mo_2N/Cudu catalyst displayed the highest one: the latter catalyst is thus more highly dispersed. This dispersion difference can be related with the concentration of oxygen surface groups: lower dispersion of the Mo_2N/Pica catalyst is attributed to the relative absence of oxygen functionalities (see results of TPD analysis), which renders the surface relatively hydrophobic, hinders the access of the aqueous solution to its internal pore structure, and does not allow homogeneous radial distribution of the metal precursor within the particles of the support. Conversely, high dispersion of the Mo_2N/Cudu catalyst is obtained on the most hydrophilic support. Table 2 also shows that the Mo/C atomic ratio is not affected by an increase in the reduction time of the Mo_2N/Norit catalyst.

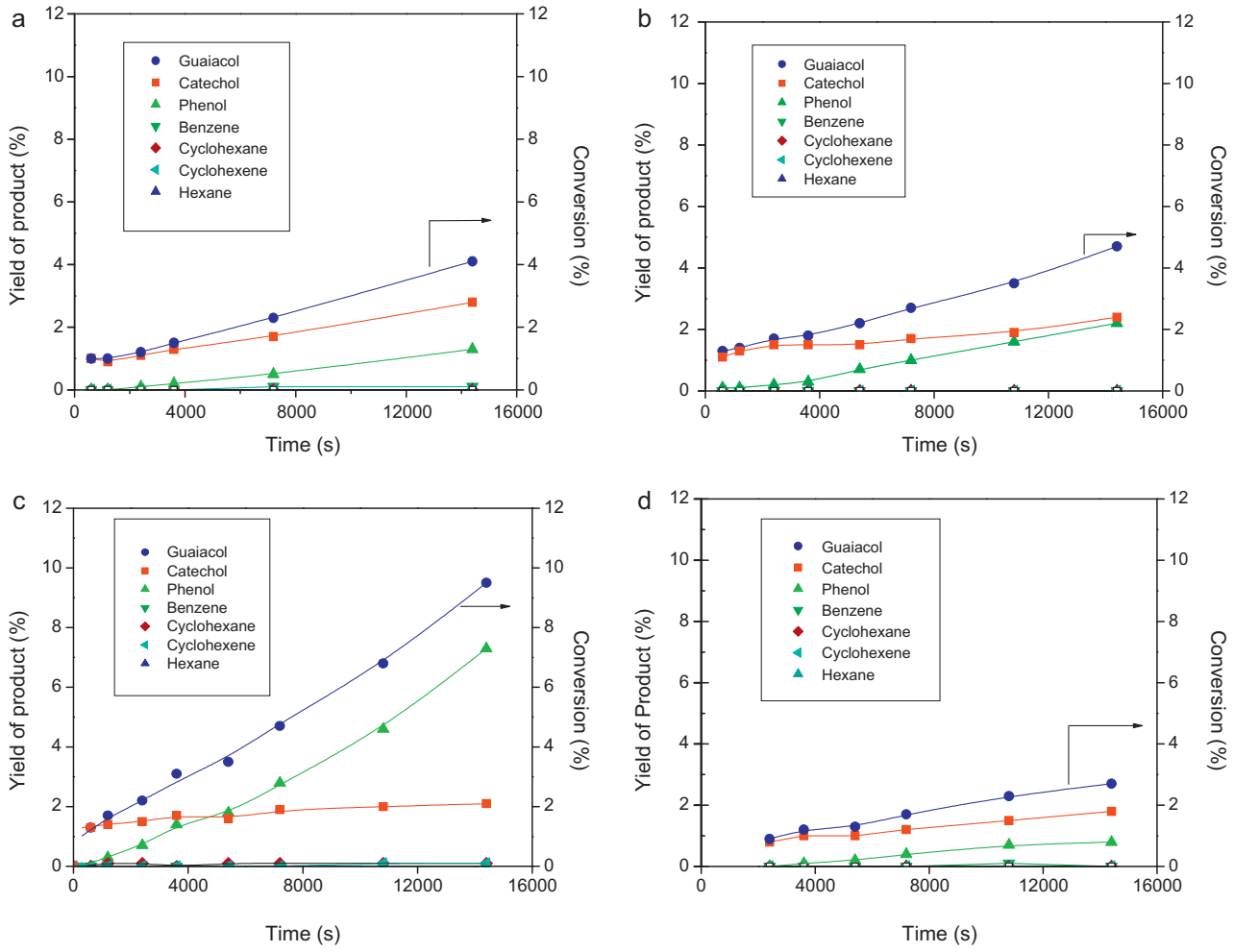

Fig. 5. Evolution of product yields and conversion of guaiacol as a function of time for: (a) unsupported Mo_2N, (b) Mo_2N/Cudu, (c) Mo_2N/Norit and (d) Mo_2N/Pica catalysts.

The Mo/N ratio in the unsupported Mo_2N catalyst was 0.81. Considering that the theoretical value is 2.0, this indicates a surface enrichment of nitrogen atoms in the active phase. Table 2 also shows that the Mo/N ratio in the Mo_2N/Cudu catalyst was even lower; therefore, it experienced an even greater degree of enrichment of surface nitrogen atoms in the active phase (or in the support). For the Mo_2N/Pica and Mo_2N/Norit catalysts such a trend could not be established due to the presence of pyrrolic groups on the support surface.

3.2. Catalytic activity

Fig. 5 shows the time evolution of product yields and guaiacol conversion for the unsupported and supported Mo_2N catalysts. In all cases the main reaction products are catechol and phenol, while the yields of benzene and cyclohexene were minor. According to the reaction scheme in Fig. 1, conversion of guaiacol to phenol can occur via two mechanisms. Guaiacol can undergo demethylation to form catechol, which is subsequently deoxygenated to form phenol. Guaiacol can also undergo demethoxylation to form phenol directly without a catechol intermediate. Based on our results, it appears that both demethylation and demethoxylation reactions occurred simultaneously. Further conversion of catechol to phenol was not prominent over the time scale used in this study, as evidenced by the continued production of catechol. Table 3 summarizes the initial rate results, which were obtained from initial slopes of the time-dependent guaiacol conversion data. The specific activity trend over the supported catalysts was Mo_2N/Pica < Mo_2N/Cudu < Mo_2N/Norit. This does not correlate with the relative dispersion values determined from the Mo/C XPS data: Mo_2N/Pica < Mo_2N/Norit < Mo_2N/Cudu. De la Puente et al. [48] have shown that an increase in the dispersion of MoS_2 on carbon supports resulted in lower HDO activity for guaiacol, ethyldecanoate, and 4-methylacetophenone. The increase in dispersion was achieved by increasing the degree of oxidation of the support, which in turn provides strong binding sites for the molybdenum precursor. Such sites were suggested to affect the catalyst surface chemistry resulting in its lower activity. A similar effect has also been reported for Co Fischer-Tropsch catalysts; below a certain particle size, activity decreases [49]. In our work, we observed *maximum* activity at intermediate relative dispersion. This suggests that controlling dispersion by optimizing support textural/chemical properties is an important parameter to investigate in these catalytic reactions using metal nitrides.

Table 3
Initial rates of reaction of all Mo_2N/carbon catalysts and Mo_2N unsupported catalyst.

Catalysts	Rate of reaction	
	$\times 10^7$ (mol g^{-1} s^{-1})	$\times 10^5$ (molecules Gua Mo $atom^{-1}$ s^{-1})
Mo_2N unsupported	0.8	–
Mo_2N/Cudu	0.9	8.75
Mo_2N/Norit	1.97	20.0
Mo_2N/Pica	0.69	7.09

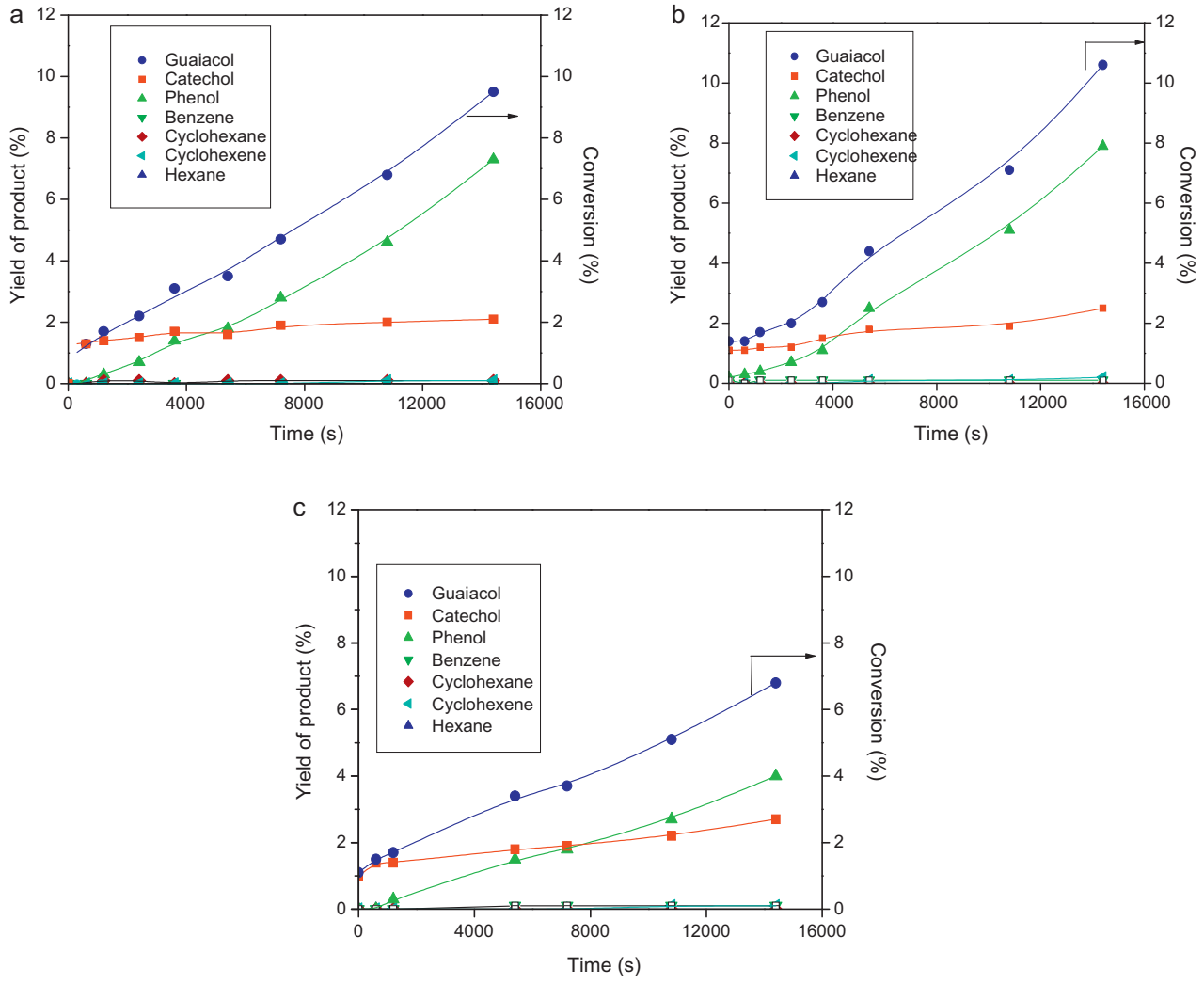

Fig. 6. Evolution of product yields and conversion of guaiacol as a function of time for: (a) Mo_2N/Norit (4 h), (b) Mo_2N/Norit (6 h) and (c) Mo_2N/Norit (8 h).

In addition, the porosity of the support has been shown to affect catalyst activity in Fischer-Tropsch synthesis [50]. Our three carbon supports had different pore size distributions and micropore/mesopore volume ratios. The Mo_2N/Norit catalyst had the lowest micropore volume fraction and the largest mesopore diameters resulting in the most open porous structure (see Table 1). The expected increase in diffusivity of reactants and products in the Mo_2N/Norit catalyst could provide another reason for the observed activity increase relative to the other catalysts.

The conversion of guaiacol was examined for the Mo_2N/Norit catalyst activated under H_2 at 400 °C for: 4, 6 and 8 h. Fig. 6 shows the evolution of reaction products for the three Mo_2N/Norit catalysts activated under different conditions. Table 4 summarizes the initial reaction rate data for these catalysts. Here, we observed a maximum in catalyst activity with a 6 h reduction time at 400 °C.

Table 4
Initial reaction rates for Mo_2N/Norit catalyst at three different reduction times.

Reduction time	Rate of reaction	
	$\times 10^7$ (mol g^{-1} s^{-1})	$\times 10^5$ (molecules Gua Mo $atom^{-1}$ s^{-1})
4 h	1.97	20.0
6 h	2.74	26.5
8 h	1.63	16.8

Increasing the reduction time beyond 6 h reduced activity. The XPS results (see Table 2) revealed an increase in the superficial abundance of Mo_2N species when the reduction time was extended from 4 to 6 h; this suggests that prolonged H_2 treatment time successfully removed the oxygen-containing surface layer formed upon catalyst passivation (see Section 2.1) and thus exposed the active Mo_2N species to the reactant stream. However, when the reduction time was further increased (beyond a critical time, which in this case was ca. 6 h), H_2 molecules were presumably successful in cleaving the Mo–N bond and forming NH_x surface species in addition to H and Mo unsaturated species. The latter can react with the available surface oxygen, either on the support or as it diffuses into the subsurface of Mo_2N species [51], thus increasing the concentration of molybdenum oxynitride species and reducing the overall HDO activity. The XPS results (see Table 2) provide circumstantial evidence for this abundance of molybdenum oxynitrides.

Fig. 7 shows the selectivity results, in terms of the phenol/cathecol ratio, calculated at 3% guaiacol conversion. The Mo_2N/Pica and Mo_2N/Cudu catalysts displayed similar selectivity, close to 0.40. However, the selectivity for the Mo_2N/Norit catalyst was higher by a factor of 2. Since the relative dispersion of the Mo_2N/Norit catalyst is between those of the Mo_2N/Pica and Mo_2N/Cudu, it is not clear at this point whether dispersion is, in part, responsible for this difference in selectivity. De la Puente, et al. [48] reported a dependency of phenol/catechol selectivity for gua-

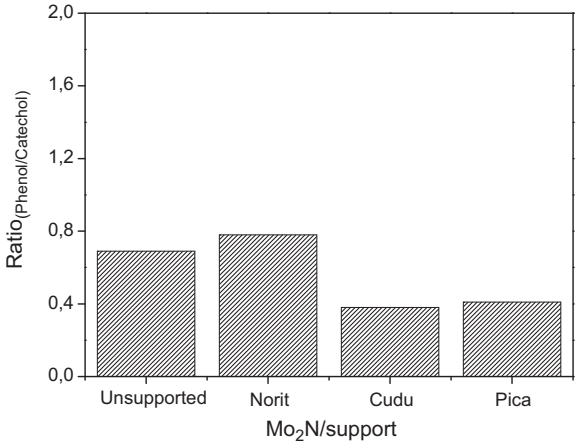

Fig. 7. Phenol/catechol ratio for nitrided catalysts.

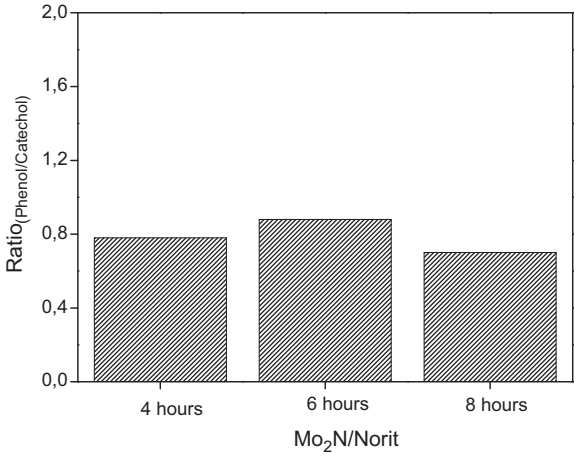

Fig. 8. Phenol/catechol ratio for Mo_2N/Norit catalysts for three different activation conditions.

iacol HDO using MoS_2/carbon catalysts synthesized under different conditions. They observed that increasing oxidation of the support prior to catalyst impregnation resulted in increased catalyst dispersion, which led to a decrease in the phenol/catechol selectivity. Our results also suggest a relationship between the dispersion of HDO catalysts and the type/quantity of active sites. Another possible explanation is the presence of impurities identified in the Norit support. Impurities such as Ti and Sr could change the electronic structure of the active sites and increase relative demethoxylation activity. Fig. 6 also shows that bulk Mo_2N displays a phenol/catechol ratio that is even higher than that of Mo_2N/Pica and Mo_2N/Cudu catalysts; this result requires further study, one possibility being that the active sites on the unsupported catalyst are somehow different from those on supported catalysts. Finally, Fig. 8 shows selectivity results for the Mo_2N/Norit catalysts prepared using different reduction times. The absence of an effect suggests that the active sites for demethylation and demethoxylation do remain the same under these conditions.

4. Conclusions

Nitrided molybdenum catalysts, either unsupported or supported on activated carbon, were active for HDO of 2-methoxyphenol. Selected commercial supports had different textural and chemical properties: (i) the Pica and Cudu carbons contained a significant fraction of micropores and the latter also had more abundant oxygen surface groups, and (ii) the Norit carbon was mainly mesoporous and had less oxygen surface functionalities than the Cudu support and more than the Pica support. The Mo_2N/Norit catalyst had the highest activity; this was attributed, in part, to its high mesoporosity, which facilitates reactant diffusion to the internal surfaces where the active sites are primarily located. Since the catalyst with the highest activity had an intermediate dispersion, our results suggest that optimizing dispersion may be important in maximizing HDO activity. Catalyst dispersion was related to the surface chemistry of the carbon support.

The Mo_2N/Norit catalyst also had the most favorable product selectivity, as measured by the phenol/cathecol ratio. The ratio of active sites for demethylation vs. demethoxylation is thus sensitive to catalyst dispersion (affecting surface properties during reaction) as well as to the presence of impurities in the support. The other two catalysts displayed similar and inferior selectivity, suggesting that the significant differences in their textural and chemical properties did not affect the nature of the Mo_2N active sites. The highest activity of the Mo_2N/Norit catalyst was obtained after 6-h reduction in H_2. This optimum is thought to be a compromise between the removal of surface oxygen that favored the formation of Mo_2N species and the formation of oxynitride species at longer times; the latter species are formed by reaction between the unsaturated Mo sites and the oxygen that is available either on the support surface or on the subsurface of the Mo_2N species. These results are encouraging and we expect promoted Mo_2N catalysts to have significantly improved activity.

Acknowledgements

Financial support for the present study was received from CONICYT Chile, projects PFB-27 and FONDECYT N° 1100512 grants. The authors also acknowledge the financial support of DOE Epscor grant #DE-FG02-07ER46373 and the technical assistance of Nick Hill.

References

[1] The Promotion of the Use of Biofuels and Other Renewable Fuels for Transport, EU Directive 2003/30/EC, 8 May, 2003.
[2] E. Laurent, B. Delmon, Ind. Eng. Chem. Res. 32 (1993) 2516.
[3] J.B. Bredenberg, M. Huuska, P. Toropainen, J. Catal. 120 (1989) 401.
[4] D.C. Elliott, G.G. Neuenschwander, in: A.V. Bridgwater, D.G.B. Boocock (Eds.), Developments in Thermochemical Biomass Conversion, vol. 1, Blackie Academic and Professional, London, 1996, p. 611.
[5] G. Guéhenneux, P. Baussand, M. Brothier, C. Poletiko, G. Boissonnet, Fuel 84 (2005) 733.
[6] E. Furimsky, Appl. Catal., A 199 (2000) 147.
[7] A.V. Bridgwater, Chem. Eng. J. 91 (2003) 87.
[8] G. Berndes, M. Hoogwijk, R. van den Broek, Biomass Bioenergy 25 (2003) 1.
[9] C. Medina, R. García, P. Reyes, J.L.G. Fierro, N. Escalona, Appl. Catal., A 373 (2010) 71.
[10] N. Escalona, C. Medina, R. García, P. Reyes, Catal. Today 143 (2009) 76.
[11] P. Ubilla, R. García, J.L.G. Fierro, N. Escalona, J. Chil. Chem. Soc. 55 (2010) 35.
[12] M.J.A. Tijmensen, A.P.C. Faaij, C.N. Hamelinck, M.R.M. van Hardeveld, Biomass Bioenergy 23 (2002) 129.
[13] K.W. Jun, H.S. Roh, K.S. Kim, J.S. Ryu, K.W. Lee, Appl. Catal., A 259 (2004) 221.
[14] A.V. Bridgwater, Appl. Catal., A 116 (1994) 5.
[15] A.V. Bridgwater, Catal. Today 29 (1996) 285.
[16] E. Laurent, B. Delmon, Appl. Catal., A 109 (1994) 77.
[17] E. Laurent, B. Delmon, Appl. Catal., A 109 (1994) 97.
[18] A. Centeno, E. Laurent, B. Delmon, J. Catal. 154 (1995) 288.
[19] M. Ferrari, S. Bosmans, R. Maggi, B. Delmon, P. Grange, Catal. Today 65 (2001) 257.
[20] V.N. Bui, G. Toussaint, D. Laurenti, C. Mirodatos, C. Geantet, Catal. Today 143 (2009) 172.
[21] P.E. Ruiz, K. Leiva, R. Garcia, P. Reyes, J.L.G. Fierro, N. Escalona, Appl. Catal., A 384 (2010) 78.
[22] N. Escalona, F.J. Gil–Llambias, M. Vrinat, T.S. Nguyen, D. Laurenti, A. López Agudo, Catal. Commun. 8 (2006) 285.
[23] G.W. Huber, S. Iborra, A. Corma, Chem. Rev. 106 (2006) 4044.
[24] W.M. Peng, Q.Y. Wu, New Energy Sources 22 (2000) 39.
[25] O.I. Senol, T.R. Viljava, A.O.I. Krause, Appl. Catal., A 326 (2007) 236.
[26] S.R.A. Kersten, W.P.M. van Swaaij, L. Lefferts, K. Seshan, in: G. Centi, R.A. va Santen (Eds.), Catalysis for Renewables – From Feedstocks to Energy Production, Wiley-VCH, Weinheim, 2007, p. 119.

[27] E. Furimsky, Appl. Catal. A: Gen. 240 (2003) 1.
[28] Y.J. Zhang, Z.B. Wei, W.H. Yan, P.L. Ying, C.X. Ji, X.S. Li, Z.H. Zhou, X.P. Sun, Q. Xin, Catal. Today 30 (1996) 135.
[29] J. Monnier, H. Sulimma, A. Dalai, G. Caravaggio, Appl. Catal., A 382 (2010) 176.
[30] J.L. Figueiredo, M.F.R. Pereira, Catal. Today 150 (2010) 2.
[31] V.H.J. de Beer, F.J. Derbyshire, C.K. Groot, R. Prins, A.W. Scaroni, J.M. Solar, Fuel 63 (1984) 1095.
[32] J. Gañán, J.P. Turegano, G. Calama, S. Roman, A. Al-Kassir, Fuel Process. Technol. 87 (2006) 117.
[33] L. Volpe, M. Boudart, J. Solid State Chem. 59 (1985) 332.
[34] U. Zielke, K. Huttinger, W. Hoffman, Carbon 34 (1996) 983.
[35] J.M. Calo, D. Cazorla- Amorós, A. Linares- Solano, M. Román-Martínez, C. Salinas- Martínez de Lecea, Carbon 35 (1997) 543.
[36] J.L. Figueiredo, M. Pereira, M. Freitas, J. Orfao, Carbon 37 (1999) 1379.
[37] C. Shi, A.M. Zhu, X.F. Yang, C.T. Au, Appl. Catal., A 276 (2004) 223.
[38] A. Lippitz, Th. Hübert, Surf. Coat. Technol. 200 (2005) 250.
[39] N. Escalona, J. Ojeda, M. Yates, A. López Agudo, J.L.G. Fierro, F.J. Gil Llambías, Appl. Catal., A 240 (2003) 151.
[40] J.P.R. Vissers, S.M.A. Bouwens, V.H.J. de Beer, R. Prins, Carbon 25 (1987) 485.
[41] S. Biniak, G. Szymanki, J. Siedlewski, A. Swiatkowski, Carbon 35 (1997) 1799.
[42] S.D. Gardner, S. Chakravarthy, K. Singamsetty, G.L. Booth, G.-R. He, Carbon 33 (1995) 587.
[43] E. Riedo, F. Comin, J. Chevrier, F. Schmithusen, S. Decossas, M. Sancrotti, Surf. Coat. Technol. 125 (2000) 124.
[44] E. D'Anna, M.L. De Giorgi, A. Luches, M. Martino, A. Perrone, A. Zocco, Thin Solid Films 347 (1999) 72.
[45] I. Takano, S. Isobe, T.A. Sasaki, T. Baba, Appl. Surf. Sci. 37 (1989) 25.
[46] K.W. Vogt, L.A. Naugher, P.A. Kohl, Thin Solid Films 256 (1995) 106.
[47] A. Chowdhury, D.C. Cameron, M.S.J. Hashmi, Surf. Coat. Technol. 112 (1999) 133.
[48] G. De la Puente, A. Gil, J.J. Pis, P. Grange, Langmuir 15 (1999) 5800.
[49] J.P. den Breejen, P.B. Radstake, G.L. Bezemer, J.H. Bitter, V. Froseth, A. Holmen, K.P. de Jong, J. Am. Chem. Soc. 131 (2009) 7197.
[50] A.M. Saib, M. Claeys, E. van Steen, Catal. Today 71 (2002) 395.
[51] Z. Wei, Q. Xin, P. Grange, B. Delmon, J. Catal. 168 (1997) 176.